

# Learning a Dilated Residual Network for SAR Image Despeckling

*Qiang Zhang<sup>[1]</sup>, Qiangqiang Yuan<sup>[1]\*</sup>, Jie Li<sup>[3]</sup>, Zhen Yang<sup>[2]</sup>, Xiaoshuang Ma<sup>[4]</sup>,*

*Huanfeng Shen<sup>[2]</sup>, Liangpei Zhang<sup>[5]</sup>*

<sup>[1]</sup> *School of Geodesy and Geomatics, Wuhan University, P. R. China*

<sup>[2]</sup> *School of Resource and Environmental Science, Wuhan University, P. R. China*

<sup>[3]</sup> *International School of Software, Wuhan University, P. R. China*

<sup>[4]</sup> *School of Resources and Environmental Engineering, Anhui University, P. R. China*

<sup>[5]</sup> *State Key Laboratory of Information Engineering, Survey Mapping and Remote Sensing, Wuhan University, P. R.*

*China*

## Abstract

In this letter, to break the limit of the traditional linear models for synthetic aperture radar (SAR) image despeckling, we propose a novel deep learning approach by learning a non-linear end-to-end mapping between the noisy and clean SAR images with a dilated residual network (SAR-DRN). SAR-DRN is based on dilated convolutions, which can both enlarge the receptive field and maintain the filter size and layer depth with a lightweight structure. In addition, skip connections are added to the despeckling model to maintain the image details and reduce the vanishing gradient problem. Compared with the traditional despeckling methods, the proposed approach shows a state-of-the-art performance in both quantitative and visual assessments, especially for strong speckle noise.

**Index Terms**—SAR image despeckling, dilated convolutions, skip connections, residual learning.

## I. INTRODUCTION

Synthetic aperture radar (SAR) is a coherent imaging sensor, which can access a wide range of high-quality massive surface data. Moreover, with the ability to operate at night and in adverse weather conditions such as thin clouds and

haze, SAR has gradually become a significant source of remote sensing data in the fields of geographic mapping, resource surveying, and military reconnaissance. However, SAR images are inherently affected by multiplicative noise, i.e., speckle noise, which is caused by the coherent nature of the scattering phenomena [1]. The presence of speckle severely affects the quality of SAR images, and greatly reduces the utilization efficiency in SAR image interpretation, retrieval, and other applications [2]–[4]. As a result, SAR image speckle reduction is an essential preprocessing step and has become a hot research topic.

For the purpose of removing the speckle noise of SAR images, researchers first proposed spatial linear filters such as the Lee filter [5] and Kuan filter [6]. These methods usually assume that the image filtering result values have a linear relationship with the original image. However, due to the nature of local processing, the spatial linear filter methods often fail to preserve edges and details.

Aimed at solving this problem, the nonlocal means (NLM) algorithm [7]–[9] has provided a breakthrough in detail preservation in SAR image despeckling. The basic idea of the NLM-based methods is that natural images have self-similarity and there are similar patches repeating over and over throughout the whole image. For instance, the SAR-BM3D algorithm [9] uses the local linear minimum mean square error (MMSE) criterion and undecimated wavelet transform and has become one of the most effective SAR despeckling methods. However, the low computational efficiency of the similar patch searching restricts its application.

In addition, the variational methods [10] have gradually been utilized for SAR image despeckling because of their stability and flexibility. The despeckling task is cast as the inverse problem of recovering the original noise-free image based upon reasonable assumptions or prior knowledge of the noise observation model. Although these variational methods [11]–[13] have achieved good reduction of speckle noise, the result is usually dependent on the choice of the model parameters and prior models.

In general, although a lot of SAR despeckling methods have been proposed, they sometimes fail to preserve sharp features in domains of complicated texture, or even create some block artifacts in the speckled image. In this letter,

considering that image speckle noise can be expressed more accurately through non-linear models than linear models, and to overcome the aforementioned limitations of the linear models, we propose a novel deep neural network based approach for SAR image despeckling, learning a non-linear end-to-end mapping between the speckled and clean SAR images by a dilated residual network (SAR-DRN). Our despeckling model employs dilated convolutions [15], which can both enlarge the receptive field and maintain the filter size and layer depth with a lightweight structure. Furthermore, skip connections are added to the despeckling model to maintain the image details and avoid the vanishing gradient problem. Compared with the traditional despeckling methods in both simulated and real SAR experiments, the proposed approach shows a state-of-the-art performance in both quantitative and visual assessments, especially for strong speckle noise.

The rest of this letter is organized as follows. The SAR image speckling noise degradation model and the related deep neural network method are introduced in Section II. The network architecture of the proposed SAR-DRN is described in Section III. The results of the despeckling assessment in both simulated and real SAR image experiments are presented in Section IV. Finally, the conclusions and future research are summarized in Section V.

## II. RELATED WORK

### A. SAR Image Speckling Noise Degradation Model

For SAR images, the main reason for the degradation of the image quality is multiplicative speckle noise. Differing from additive white Gaussian noise (AWGN), speckle noise is described by the multiplicative noise model:

$$y = x \cdot n \tag{1}$$

where  $y$  is the speckle noise image,  $x$  is the clean image, and  $n$  represents the probability distribution of the speckle noise, whose expectation and standard deviation are 1 and  $\sigma$ . It should be noted that speckle follows a gamma distribution [13]:

$$\rho_n(n) = \frac{L^L n^{L-1} \exp(-nL)}{\Gamma(L)} \tag{2}$$

where  $L \geq 1$ ,  $n \geq 0$ ,  $\Gamma$  is the gamma function, and  $L$  is the equivalent number of looks (ENL), as defined in (3), which is usually regarded as the quantitative evaluation index for real SAR image despeckling experiments.

$$ENL = \frac{mean^2}{std^2} \quad (3)$$

where  $mean$  and  $std$  respectively represent the image mean and standard deviation.

Therefore, for this non-linear gamma multiplicative noise, choosing a non-linear expression for speckle reduction is an important strategy. In the following, we briefly introduce the use of convolutional neural networks (CNNs) for SAR image despeckling, considering both the low-level features as the bottom level and the output feature representation from the top level of the network.

## ***B. CNNs for SAR Image Despeckling***

Recently, benefiting from the powerful non-linear expression of deep convolution neural networks (DCNNs), CNNs have gradually become an efficient image processing method which has been successfully applied to many computer vision tasks such as image classification, segmentation, object recognition, and so on [24]–[25]. CNNs can extract the image internal features and avoid the complex preprocessing of images, organized in a feature map of  $m_1 \times n_1 \times c_1$ , within which each unit is connected to local patches of the previous layer through a set of weight parameters  $W$  of size  $k_1 \times k_2 \times N$  and bias parameters  $b$ . The output feature map is:

$$f^s = \sum_{i=1}^N W_i^s * x^i + b^s \quad (4)$$

where  $*$  is a two-dimensional discrete convolution operation,  $f^s$  is the output feature map of size  $m_2 \times n_2 \times c_2$ , and  $x^i$  is the  $i$ -th input feature map. Specially, the network parameters  $W$  and  $b$  need to be regenerated through back-propagation and the chain rule of derivation.

To ensure that the output of the CNN is a non-linear combination of the input, a non-linear function is introduced as an excitation function, such as the rectified linear unit (ReLU):

$$z^s = \max(0, f^s) \quad (5)$$

For natural Gaussian noise reduction, a new method named the feed-forward denoising convolutional neural network (DnCNN) [13] has recently shown excellent performances, in contrast with the traditional methods which employ a deep convolutional neural network. DnCNN employs a 20 convolutional layers structure, a learning strategy of residual learning, and an output data regularization method of batch normalization.

On the basis of [14], the SAR-CNN method [16] also employs a set of convolutional layers, along with batch normalization (BN) [17] and a ReLU activation function, and a component-wise division residual layer to estimate the speckled image, as shown in Fig. 1. As an alternative way of dealing with the multiplicative noise of SAR images, SAR-CNN uses the homomorphic approach with coupled logarithm and exponent transforms in combination with a similarity measure for speckle noise distribution.

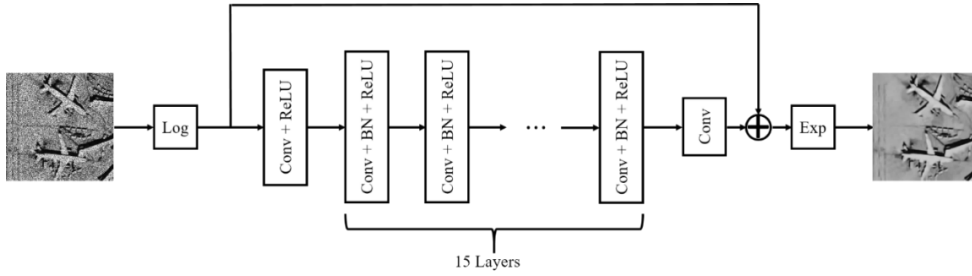


Fig. 1. The architecture of SAR-CNN [16].

### III. PROPOSED METHOD

In this letter, rather than using log transform or modifying the loss function, we propose a novel network called SAR-DRN, which is trained in an end-to-end fashion using a combination of dilated convolutions and skip connections. Instead of relying on pre-determined image *a priori* knowledge or a noise description model, the main superiority of using the deep neural network strategy for SAR image despeckling is that the model can directly acquire and update the network parameters from the training data and the corresponding labels.

The proposed holistic neural network model (SAR-DRN) for SAR image despeckling contains seven dilated convolution layers and two skip connections, as illustrated in Fig. 2. In addition, the proposed model uses a residual learning strategy to predict the speckled image, which adequately utilizes the non-linear expression ability of deep

learning. The details of the algorithm are described in the following.

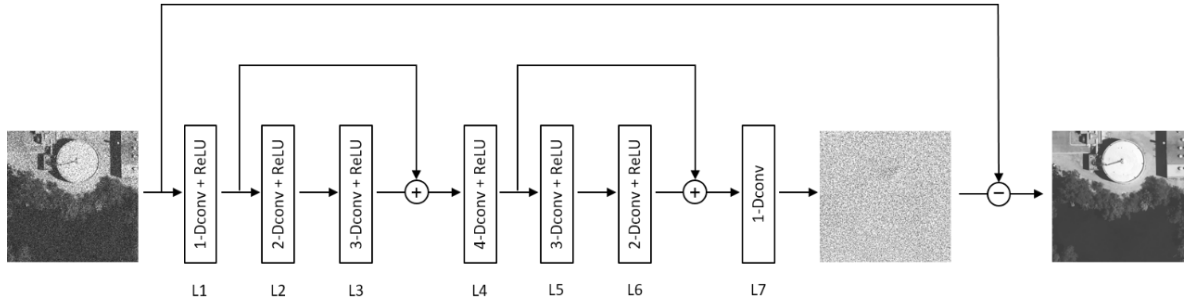


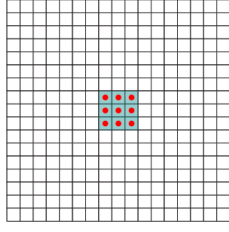
Fig. 2. The architecture of the proposed SAR-DRN.

### A. Dilated Convolutions

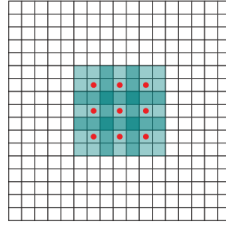
In image restoration problems such as single-image super-resolution (SISR) and denoising and deblurring, contextual information can effectively facilitate the recovery of degraded regions. In deep convolutional networks, they mainly augment the contextual information through enlarging the receptive field. Generally speaking, there are two ways to achieve this purpose: 1) increasing the network depth; and 2) enlarging the filter size. Nevertheless, as the network depth increases, the accuracy becomes “saturated” and then degrades rapidly. Enlarging the filter size can also lead to more convolution parameters, which greatly increases the calculative burden and training times.

To solve this problem effectively, dilated convolutions were first proposed in [15], which is an approach that can both enlarge the receptive field and maintain the filter size. Setting kernel size=3×3 as an example, Fig. 3 illustrates the dilated convolution receptive field size, where: (a) corresponds to the 1-dilated convolution, which is equivalent to the common convolution operation at this point; (b) corresponds to the 2-dilated convolution; and (c) corresponds to the 4-dilated convolution. The common convolution receptive field has a linear correlation with the layer depth, in that the receptive field size  $F_{depth-i} = (2i+1) \times (2i+1)$ , while the dilated convolution receptive field has an exponential correlation with the layer depth, where the receptive field size  $F_{depth-i} = (2^{i+1} - 1) \times (2^{i+1} - 1)$ .

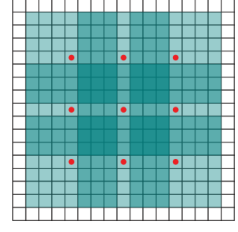
In the proposed model, the dilation factors of the 3×3 dilated convolutions from layer 1 to layer 7 are respectively set to 1, 2, 3, 4, 3, 2, and 1. Compared with other deep networks, we propose a lightweight model with only seven dilated convolution layers, as shown in Fig. 2.



(a) 1-dilated convolution



(b) 2-dilated convolution



(c) 4-dilated convolution

Fig. 3. Dilated convolution receptive field size.

## B. Skip Connections

Although the increase of network layer depth can help to obtain more data feature expressions, it often results in the vanishing gradient problem, which makes the training of the model much harder. To solve this problem, a new structure called skip the connection [19] has been created for the DCNNs. The skip connection can pass the previous layer's feature information to its posterior layer, maintaining the image details and avoiding or reducing the vanishing gradient problem. In the proposed model, two skip connections are employed to connect layer 1 to layer 3 (as shown in Fig. 2) and layer 4 to layer 7.

## C. Residual Learning

Compared with traditional data mapping, He *et al.* [18] found that residual mapping can acquire a more effective learning effect and rapidly reduce the loss after passing through a multi-layer network. It is reasonable to consider that most pixel values in residual image  $\phi$  are very close to zero, and the spatial distribution of the residual feature maps should be very sparse, which can transfer the gradient descent process to a much smoother hyper-surface of loss to filtering parameters. Thus, searching for an allocation which is on the verge of the optimal for the network's parameters becomes much quicker and easier, allowing us to add more layers to the network and improve its performance.

Specifically, given a collection of  $N$  training image pairs  $\{x_i, y_i\}_N$ ,  $y_i$  is the gamma noisy image,  $x_i$  is the clean image, and  $\Theta$  is the network parameters. Our model uses the mean squared error (MSE) as the loss function:

$$loss(\Theta) = \frac{1}{2N} \sum_{i=1}^N \|\phi(y_i, \Theta) - (y_i - x_i)\|_2^2 \quad (6)$$

In summary, with the dilated convolutions and skip connections structure, the flowchart of learning a deep network for the SAR image despeckling process is described in Fig. 4.

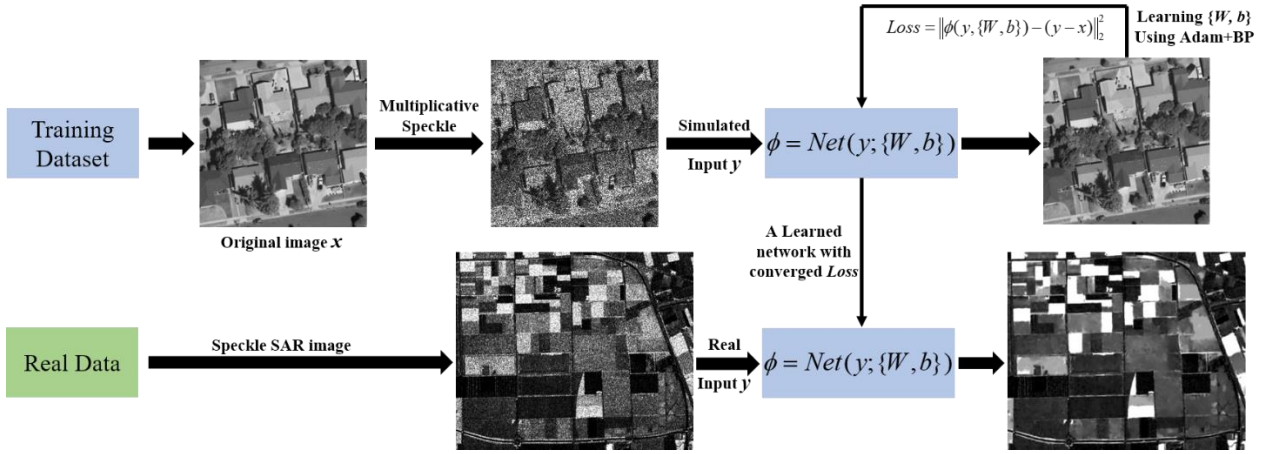


Fig. 4. The framework of SAR image despeckling based on deep learning.

## IV. EXPERIMENTAL RESULTS AND ANALYSIS

### A. Implementation Details

- 1) **Training and Test Datasets:** For SAR image despeckling with different numbers of looks, we used the UC Merced land-use dataset [20] as our training dataset, which contains 21 scene classes with 100 images per class. To train the proposed SAR-DRN, we chose 400 images of size  $256 \times 256$  from this dataset and set each patch size as  $40 \times 40$  and stride=10. We then cropped  $1513 \times 128$  patches for training SAR-DRN. The number of looks  $L$  was set to noise levels of 1, 2, 4, 8, and 16. To test the performance of the proposed model, single examples of the Airplanes and Buildings classes were respectively set up as simulated images. For the real SAR image despeckling, we used the classic Flevoland SAR image (cropped to  $500 \times 600$ ), which is commonly used in real SAR data image despeckling.
- 2) **Parameter Setting and Network Training:** Table I lists the parameters of each layer for SAR-DRN. The proposed model was trained using the Adam [21] algorithm as the gradient descent optimization method, with momentum1=0.9 and momentum2=0.999, where the learning rate was initialized to 0.01 for the whole network. The training process of SAR-DRN took 50 epochs, and after every 10 epochs, the learning rate was reduced through being multiplied by a descending factor  $\gamma = 0.5$ . We used Caffe [22] to train the proposed SAR-DRN in the Windows 7 environment, with an Intel Xeon E5-2609 v3 CPU at 1.90 GHz and an Nvidia Titan-X (Pascal) GPU.

TABLE I

THE NETWORK CONFIGURATION OF SAR-DRN

	Configurations
Layer 1	Dilated Conv + ReLU: $1 \times 64 \times 3 \times 3$ , dilate=1, stride=1, pad=1
Layer 2	Dilated Conv + ReLU: $64 \times 64 \times 3 \times 3$ , dilate=2, stride=1, pad=2
Layer 3	Dilated Conv + ReLU: $64 \times 64 \times 3 \times 3$ , dilate=3, stride=1, pad=3
Layer 4	Dilated Conv + ReLU: $64 \times 64 \times 3 \times 3$ , dilate=4, stride=1, pad=4
Layer 5	Dilated Conv + ReLU: $64 \times 64 \times 3 \times 3$ , dilate=3, stride=1, pad=3
Layer 6	Dilated Conv + ReLU: $64 \times 64 \times 3 \times 3$ , dilate=2, stride=1, pad=2
Layer 7	Dilated Conv: $64 \times 1 \times 3 \times 3$ , dilate=1, stride=1, pad=1

**3) Compared Algorithms and Quantitative Evaluations:** To verify the proposed method, we compared SAR-DRN with five other despeckling methods: The Lee filter [5], the probabilistic patch-based (PPB) filter [8], SAR-BM3D [9], SAR-POTDF [13], and SAR-CNN [16]. In the simulated-image experiments, the peak signal-to-noise ratio (PSNR) and structural similarity (SSIM) were employed as the quantitative evaluation indexes. In the real-image experiments, the ENL was considered as the smoothness of a homogeneous region after SAR image despeckling (the ENL is commonly regarded as the quantitative evaluation index for real SAR image despeckling experiments).

### B. Simulated-Data Experiments

To verify the effectiveness of the proposed SAR-DRN model in SAR image despeckling, five speckle noise levels of  $L=1, 2, 4, 8,$  and  $16$  were set up for the two simulated images. The PSNR and SSIM results of the simulated experiments with the two images are listed in Table III and Table IV, where the best performance is marked in bold and the second-best performance is underlined.

Table II  
PSNR (DB) RESULTS FOR AIRPLANE AND BUILDING

Looks	Airplane					Building				
	L=1	L=2	L=4	L=8	L=16	L=1	L=2	L=4	L=8	L=16
Noisy	10.2101	12.9891	15.9128	18.9256	21.9060	13.9613	16.6655	19.6683	22.5580	25.5763
Lee	17.2951	20.2395	22.9602	25.1767	27.4167	21.0689	24.1271	26.8257	28.9741	31.0374
PPB	20.0131	21.7464	23.4926	25.0114	26.3038	25.0664	26.3441	28.0539	29.4994	30.9134
SAR-BM3D	<u>21.8878</u>	23.6551	25.4901	27.1588	28.8698	<u>26.1848</u>	<u>27.9609</u>	<u>29.8702</u>	31.3759	33.0436
SAR-POTDF	21.7304	<u>23.9854</u>	<u>25.8604</u>	<u>27.5737</u>	29.1159	24.8107	27.4031	29.5543	<u>31.5631</u>	<u>33.7106</u>
SAR-CNN	21.6321	23.6394	25.7899	27.0906	<u>29.7932</u>	25.1873	27.1438	29.3698	30.8542	33.7578
Proposed	<b>22.9720</b>	<b>24.5428</b>	<b>26.5209</b>	<b>28.0165</b>	<b>29.9986</b>	<b>26.8098</b>	<b>28.3951</b>	<b>30.1478</b>	<b>32.0322</b>	<b>33.8064</b>

Table III  
SSIM Results for Airplane and Building

Looks	Airplane					Building				
	L=1	L=2	L=4	L=8	L=16	L=1	L=2	L=4	L=8	L=16
Noisy	0.2249	0.3016	0.3926	0.4962	0.6036	0.2312	0.3386	0.5692	0.5960	0.7127
Lee	0.5676	0.5683	0.6628	0.7456	0.8129	0.6044	0.7013	0.7849	0.8387	0.8850
PPB	0.5159	0.5972	0.6786	0.7424	0.7902	0.7179	0.7809	0.8358	0.8706	0.8981
SAR-BM3D	<u>0.6242</u>	<u>0.6964</u>	<u>0.7566</u>	<u>0.8023</u>	0.8430	<u>0.7888</u>	<u>0.8352</u>	<b>0.8807</b>	<b>0.9049</b>	0.9276
SAR-POTDF	0.6062	0.6857	0.7513	0.7940	0.8297	0.7284	0.8121	0.8640	0.9013	<u>0.9291</u>
SAR-CNN	0.5831	0.6807	0.7486	0.7822	<u>0.8469</u>	0.7067	0.7804	0.8492	0.8749	0.9286
Proposed	<b>0.6579</b>	<b>0.7279</b>	<b>0.7636</b>	<b>0.8203</b>	<b>0.8471</b>	<b>0.7974</b>	<b>0.8381</b>	<u>0.8712</u>	<u>0.9022</u>	<b>0.9327</b>

As shown in Table II and Table III, the proposed SAR-DRN model obtains all the best PSNR results and three of the five best SSIM results in the five noise levels. When L=1, the proposed method outperforms SAR-BM3D by about 1.1 dB and 0.6 dB for Airplane and Building, respectively. When L=2 and 4, SAR-DRN outperforms SAR-POTDF, SAR-BM3D, and SAR-CNN by at least 0.5 dB/0.7 dB and 0.4 dB/0.3 dB for Airplane/Building, respectively. Compared with the traditional despeckling methods, the proposed approach shows a state-of-the-art performance in both the quantitative and visual assessments, especially for strong speckle noise.

Fig. 5 and Fig. 6 correspondingly show the filtered images for the Airplane and Building images contaminated by 2-look speckle and 4-look speckle, respectively. For the result of the Lee filter, there is still much speckle noise that is not completely removed. It can be seen that PPB has a better speckle-reduction ability than the Lee filter, but PPB simultaneously creates many texture distortions, especially around the edges of the airplane and building. SAR-BM3D and SAR-POTDF perform better than PPB on both the Airplane and Building images, especially for strong speckle noise such as L=1 or 2, which reveals an excellent speckle-reduction ability and local detail preservation ability. Furthermore, they generate fewer texture distortions, as shown in Fig. 6 and Fig. 7. However, SAR-BM3D and SAR-POTDF also simultaneously result in over-smoothing, to some degree, as they mainly concentrate on some complex geometric features. SAR-CNN also shows a good speckle-reduction ability and local detail preservation ability, but it introduces many radiation distortions in homogeneous regions. Compared with the other algorithms, SAR-DRN achieves the best performance in speckle reduction, concurrently avoiding introducing radiation and geometric

distortion. In addition, from the red boxes of the Airplane and Building images in Figs. 5 and 7, respectively, it can be clearly seen that SAR-DRN also shows the best local detail preservation ability, while the other methods either miss partial texture details or produce blurry results, to some extent.

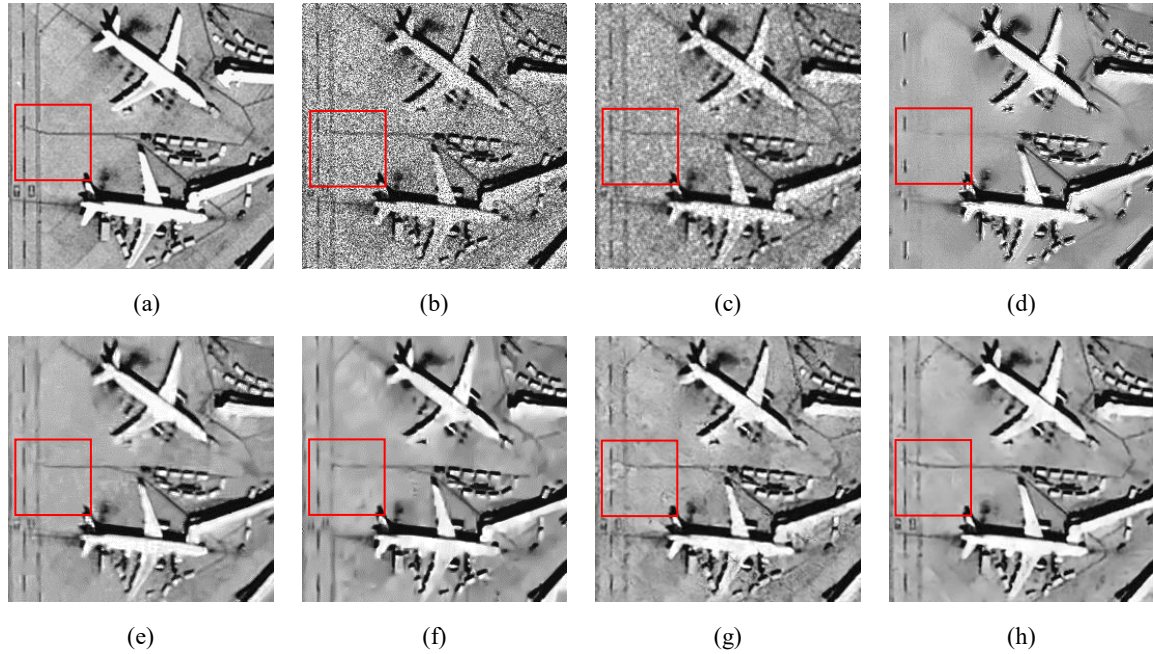


Fig. 5. Filtered images for the Airplane image contaminated by 2-look speckle. (a) Original image. (b) Speckled image. (c) Lee filter [5]. (d) PPB [8]. (e) SAR-BM3D [9]. (f) SAR-POTDF [13]. (g) SAR-CNN [16]. (h) SAR-DRN

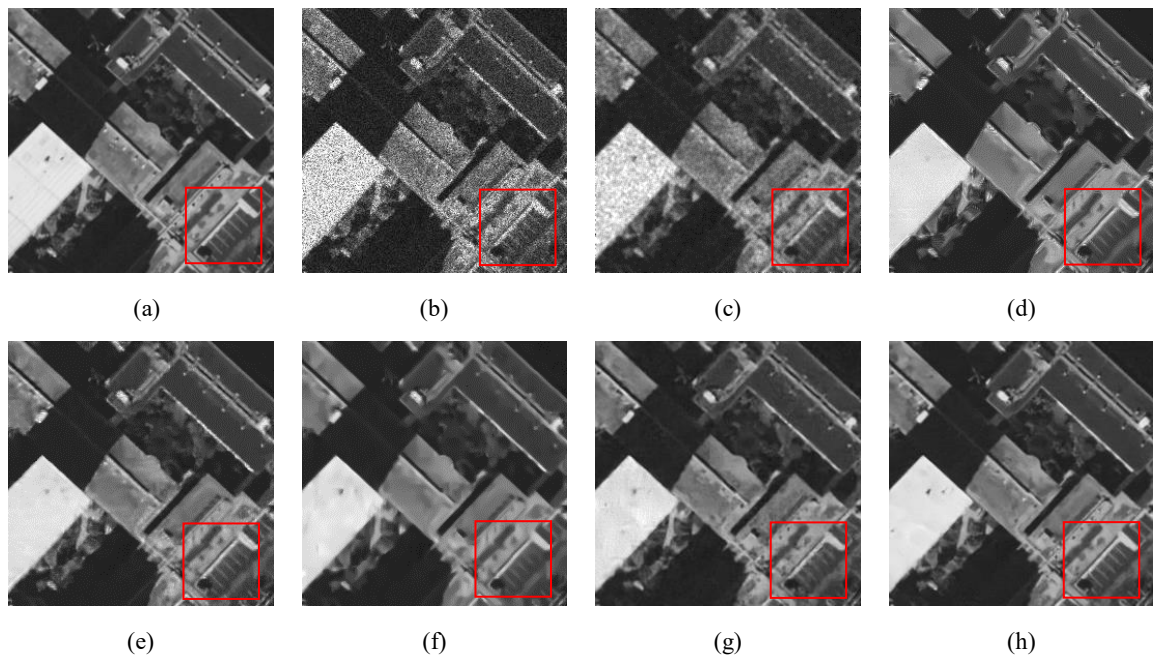


Fig. 6. Filtered images for the Building image contaminated by 4-look speckle. (a) Original image. (b) Speckled image. (c) Lee filter [5]. (d) PPB [8]. (e) SAR-BM3D [9]. (f) SAR-POTDF [13]. (g) SAR-CNN [16]. (h) SAR-DRN.

### C. Real-Data Experiments

As shown in Fig. 7, we also compared the proposed method with the four state-of-the-art methods described above on a real SAR image. It can be clearly seen that the result of SAR-BM3D still contains a great deal of residual speckle noise, while the results of PPB, SAR-POTDF, SAR-CNN, and the proposed SAR-DRN method reveal good speckle-reduction ability. PPB performs very well in speckle reduction, but it generates a few texture distortions in the edges of prominent objects. In homogeneous regions, SAR-POTDF does not perform as well in speckle reduction as the proposed SAR-DRN. As for SAR-CNN, its edge-preserving ability is weaker than that of SAR-DRN. Visually, SAR-DRN achieves the best performance in speckle reduction and local detail preservation, performing better than the other mainstream methods.

In addition, we also evaluated the filtered results through ENL to measure the speckle-reduction ability. The ENL values were estimated from two chosen homogeneous regions (the red boxes in Fig. 8(a)) and are listed in Table IV. Clearly, SAR-DRN has a much better speckle-reduction ability than the other methods, which is consistent with the visual observation.

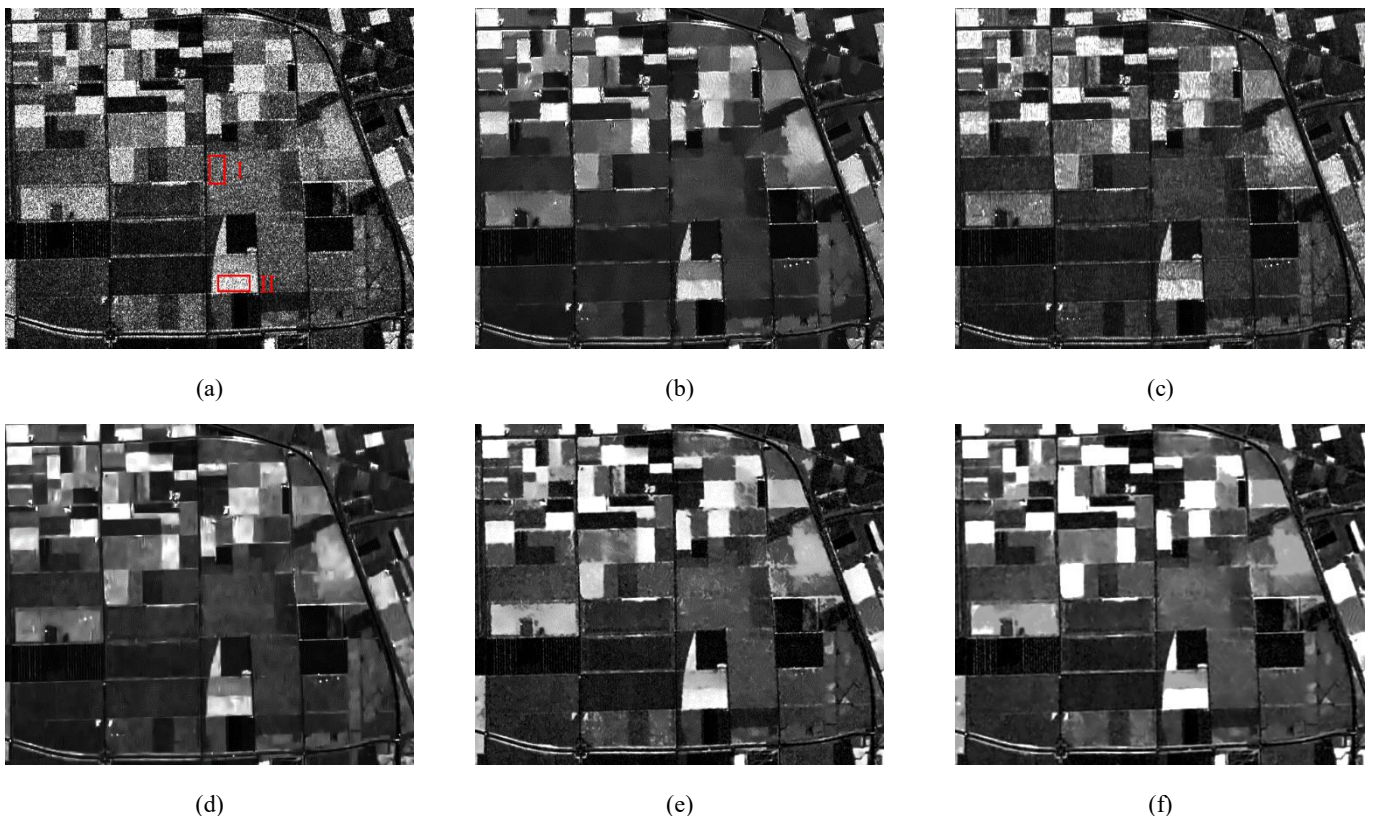


Fig. 7. Filtered images for the Building image contaminated by 4-look speckle. (a) Original image. (b) PPB [8]. (c) SAR-BM3D [9]. (d) SAR-POTDF [13]. (e) SAR-CNN [16]. (f) SAR-DRN.

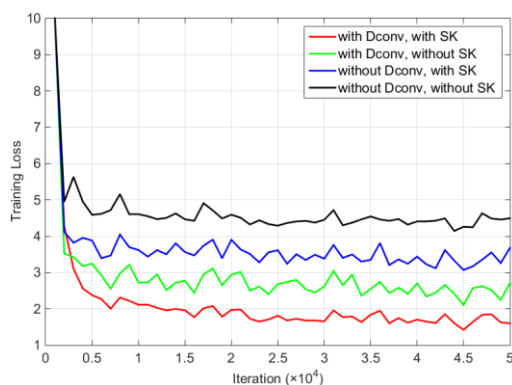
TABLE IV  
ENL RESULTS FOR THE FLEVOLAND IMAGE

Method	PPB	SAR-BM3D	SAR-POTDF	SAR-CNN	SAR-DRN
--------	-----	----------	-----------	---------	---------

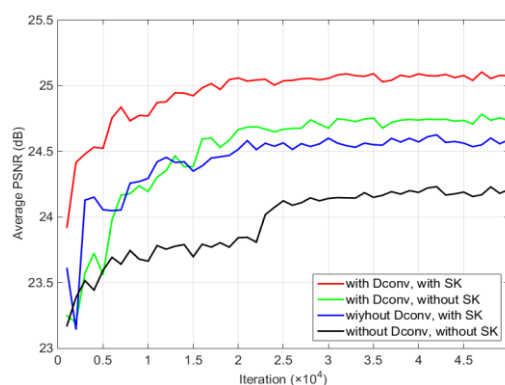
Region I	105.2469	39.1763	140.3258	118.2997	<b>171.6375</b>
Region II	125.3481	63.2657	154.9074	186.3829	<b>234.8743</b>

## D. Discussion

**1) Dilated Convolutions and Skip Connections:** To verify the effectiveness of the dilated convolutions and skip connections, we implemented four sets of experiments in the same environment as that shown in Fig. 8: 1) with dilated convolutions and skip connections (the red line); 2) with dilated convolutions but without skip connections (the green line); 3) without dilated convolutions but with skip connections (the blue line); and 4) without dilated convolutions and skip connections (the black line).



(a) Training loss



(b) Average PSNR

Fig. 8. The simulated SAR image despeckling results of the four specific models in (a) training loss and (b) average PSNR, with respect to iterations. The four specific models were different combinations of dilated convolutions (**Dconv**) and skip connections (**SK**), and were trained with 1-look images in the same environment. The results were evaluated on the *Set14* [23] dataset.

As Fig. 8 implies, the dilated convolutions can effectively reduce the training loss and enhance the despeckling performance (PSNR). Meanwhile, the skip connections also accelerate the convergence speed of the network and enhance the model stability.

**2) With or Without Batch Normalization (BN) in the Network:** Unlike the methods proposed in [14] and [16], which utilize batch normalization to normalize the output features, SAR-DRN does not add this preprocessing layer, considering that the skip connections can also maintain the outputs of the data distribution in the different dilated convolution layers. The quantitative comparison of the two structures for SAR image despeckling is provided in Section IV. Furthermore, getting rid of the BN layers can simultaneously reduce the amount of computation, saving about

3 hours of training time in the same environment. Fig. 9 shows that this modification improves the despeckling performance and reduces the complexity of the model. With regard to this phenomenon, we suggest that a possible reason is that the input and output have a highly similar spatial distribution for this regression problem, while the BN layers normalize the hidden layers' output, which destroys the representation of the original space, such as the gamma distribution.

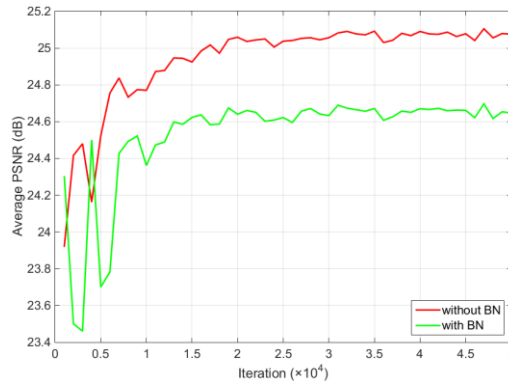


Fig. 9. The simulated SAR image despeckling results of the two specific models with/without batch normalization (BN). The two specific models were trained with 1-look images in the same environment, and the results were evaluated on the *Set14* [23] dataset.

## V. CONCLUSION

In this letter, we have proposed a novel deep learning approach for the SAR image despeckling task, learning an end-to-end mapping between the noisy and clean SAR images. The presented approach is based on dilated convolutions, which can both enlarge the receptive field and maintain the filter size with a lightweight structure. Furthermore, skip connections are added to the despeckling model to maintain the image details and avoid the vanishing gradient problem. Compared with the traditional despeckling methods, the proposed SAR-DRN approach shows a state-of-the-art performance in both simulated and real SAR image despeckling experiments, especially for strong speckle noise.

In our future work, we will investigate more powerful learning models to deal with the complex real scenes in SAR images. Furthermore, the proposed approach will be extended to polarimetric SAR image despeckling, whose noise model is much more complicated than that of single-polarization SAR.

## REFERENCES

- [1] J. W. Goodman, "Some fundamental properties of speckle," *J. Opt. Soc. Am.*, vol. 66, no. 11, pp. 1145–1150, 1976.
- [2] J. Chen, L. Jiao, and Z. Wen, "High-level feature selection with dictionary learning for unsupervised SAR imagery terrain classification," *IEEE J. Sel. Topics Appl. Earth Observ. Remote Sens.*, vol. 10, no. 1, pp. 145–160, 2017.
- [3] H. Liu, S. Yang, S. Gou, P. Chen, Y. Wang, and L. Jiao, "Fast Classification for Large Polarimetric SAR Data Based on Refined Spatial-Anchor Graph," *IEEE Geosci. Remote Sens. Lett.*, 2017.
- [4] Y. Duan, F. Liu, and L. Jiao, "Sketching Model and Higher Order Neighborhood Markov Random Field-Based SAR Image Segmentation," *IEEE Geosci. Remote Sens. Lett.*, vol. 13, no. 11, pp. 1686–1690, 2016.
- [5] J.-S. Lee, "Digital image enhancement and noise filtering by use of local statistics," *IEEE Trans. Pattern Anal. Mach. Intell.*, no. 2, pp. 165–168, 1980.
- [6] D. T. Kuan, A. A. Sawchuk, T. C. Strand, and P. Chavel, "Adaptive noise smoothing filter for images with signal-dependent noise," *IEEE Trans. Pattern Anal. Mach. Intell.*, no. 2, pp. 165–177, 1985.
- [7] A. Buades, B. Coll, and J.-M. Morel, "A non-local algorithm for image denoising," in *Proc. IEEE Computer Society Conf. Computer Vision and Pattern Recognition 2005*, vol. 2, pp. 60–65.
- [8] C. A. Deledalle, L. Denis, and F. Tupin, "Iterative weighted maximum likelihood denoising with probabilistic patch-based weights," *IEEE Trans. Image Process.*, vol. 18, no. 12, p. 2661, 2009.
- [9] S. Parrilli, M. Poderico, C. V. Angelino, and L. Verdoliva, "A nonlocal SAR image denoising algorithm based on LLMMSE wavelet shrinkage," *IEEE Trans. Geosci. Remote Sens.*, vol. 50, no. 2, pp. 606–616, 2012.
- [10] X. Ma, H. Shen, X. Zhao, and L. Zhang, "SAR image despeckling by the use of variational methods with adaptive nonlocal functionals," *IEEE Trans. Geosci. Remote Sens.*, vol. 54, no. 6, pp. 3421–3435, 2016.
- [11] Q. Yuan, L. Zhang, and H. Shen, "Hyperspectral image denoising employing a spectral–spatial adaptive total variation model," *IEEE Trans. Geosci. Remote Sens.*, vol. 50, no. 10, pp. 3660–3677, 2012.
- [12] J. Li, Q. Yuan, H. Shen, and L. Zhang, "Noise removal from hyperspectral image with joint spectral-spatial distributed sparse representation," *IEEE Trans. Geosci. Remote Sens.*, vol. 54, no. 9, pp. 5425–5439, 2016.
- [13] B. Xu *et al.*, "Patch ordering-based SAR image despeckling via transform-domain filtering," *IEEE J. Sel. Topics Appl. Earth Observ. Remote Sens.*, vol. 8, no. 4, pp. 1682–1695, 2015.

- [14] K. Zhang, W. Zuo, Y. Chen, D. Meng, and L. Zhang, "Beyond a gaussian denoiser: Residual learning of deep CNN for image denoising," *IEEE Trans. Image Process.*, 2017.
- [15] F. Yu and V. Koltun, "Multi-scale context aggregation by dilated convolutions," *arXiv preprint arXiv:1511.07122*, 2015.
- [16] G. Chierchia, D. Cozzolino, G. Poggi, and L. Verdoliva, "SAR image despeckling through convolutional neural networks," *arXiv preprint arXiv:1704.00275*, 2017.
- [17] S. Ioffe and C. Szegedy, "Batch normalization: Accelerating deep network training by reducing internal covariate shift," in *Proc. Int. Conf. Machine Learning*, 2015, pp. 448–456.
- [18] K. He, X. Zhang, S. Ren, and J. Sun, "Deep residual learning for image recognition," in *Proc. IEEE Conf. Computer Vision and Pattern Recognition*, 2016, pp. 770–778.
- [19] X. Mao, C. Shen, and Y.-B. Yang, "Image restoration using very deep convolutional encoder-decoder networks with symmetric skip connections," in *Proc. Advances in Neural Information Processing Systems*, 2016, pp. 2802–2810.
- [20] Y. Yang and S. Newsam, "Bag-of-visual-words and spatial extensions for land-use classification," in *Proc. 18th SIGSPATIAL Int. Conf. Advances in Geographic Information Systems*, 2010, pp. 270–279.
- [21] D. Kingma and J. Ba, "Adam: A method for stochastic optimization," *arXiv preprint arXiv:1412.6980*, 2014.
- [22] Y. Jia *et al.*, "Caffe: Convolutional architecture for fast feature embedding," in *Proc. 22nd ACM Int. Conf. Multimedia*, 2014, pp. 675–678.
- [23] R. Zeyde, M. Elad, and M. Protter, "On Single Image Scale-Up Using Sparse-Representations," in *Int. Conf. on Curves and Surfaces*, 2010, pp. 711-730.
- [24] L. Zhang, L. Zhang, and B. Du, "Deep Learning for Remote Sensing Data: A Technical Tutorial on the State of the Art," *IEEE Geoscience and Remote Sensing Magazine*, vol. 4, no. 2, pp. 22-40, 2016.
- [25] G. S. Xia *et al.*, "AID: A Benchmark Data Set for Performance Evaluation of Aerial Scene Classification," *IEEE Trans. Geosci. Remote Sens.*, vol. PP, no. 99, pp. 1-17, 2016.